Measured Blockage Effect of a Finger and Similar Small Objects at 300 GHz

Pekka Kyösti*†, Nuutti Tervo*, Markus Berg*‡, Marko E. Leinonen*, Klaus Nevala*, Aarno Pärssinen*
*Centre for Wireless Communications, University of Oulu
†Keysight Technologies, Oulu, Finland, ‡ExcellAnt, Oulu, Finland
pekka.kyosti@oulu.fi

***Abstract*—We study the effect of a finger, and other objects with similar shape, on the channel gain in short distance propagation measurements at 220–330 GHz. Channel impulse responses and channel gains of six objects are analyzed on different positions obstructing a 35 cm line of sight (LOS) link. The intention is to evaluate potential user effects on portable devices supporting the future 6G system. Very short wavelength and link distance cause strong fluctuation of channel gain even on millimetre scale movement of obstacles. The finger phantom causes 44 dB attenuation on close vicinity, 5 mm, of transmitter antenna and has similar attenuation pattern with corresponding metallic stripes. On the contrary, it is observed that some objects, such as the measured Nylon rod, may even increase the signal strength. These impacts are important when studying the wave propagation and network aspects of high frequencies systems.**

***Index Terms*—Terahertz, blockage, diffraction, propagation, measurements.**

I. Introduction

Fifth generation (5G) networks and devices are already in the commercial roll-out phase and the research community has started moving the focus towards sixth generation (6G). An important driver for this is the same as in the past, namely the need for higher data rates. This time, the ultimate goal is set to 1 Tbps [1]. The need of extremely wide bandwidth is pushing the research towards higher frequencies due to the limited availability of the frequency bands below 100 GHz. Several research projects are ongoing or initiated aiming to utilize upper millimetre wave (mm-wave) band at 100–300 GHz and THz bands above 300 GHz. Also standardization activities such as in [2] have taken the first steps.

Propagation channel is a fundamental component of wireless communication systems. Characterization of radio channel in considered environments and frequencies is necessary when studying and developing the future systems. Previous generation channel models at below 6 GHz were developed by using time continuous and phase coherent data measured by channel sounders that utilize high number of transmitter (Tx) and receiver (Rx) antennas. However, channel measurements become more difficult at higher frequencies as compared to below 6 GHz channel sounding. Firstly, the propagation loss is higher and must be compensated by directive high gain measurement antennas. Secondly, the phase coherence between RF chains and even temporal measurements is much more challenging to maintain. Channel characterization for lower mm-wave frequencies is discussed in [3]. The challenges of mm-wave sounding are even greater at upper mm-wave and THz. The literature shows that the majority of channel measurements above 100 GHz have been performed by using network analyzer based measurement setups. The used link distances are limited by radio frequency (RF) cables connecting the antennas, frequency extenders, and the measurement equipment. The measurement time of a single link may be up to tens of hours due to the rotating antennas, slow frequency sweeps, and polarization turns [4]. Hence, the measurements are aimed for a static channel with few measurement locations.

Fortunately, the potential use-cases for the 6G system at upper mm-wave are mainly targeted to indoor and LOS scenarios with limited link distances. A high resolution measurement in angular, polarization and delay domains, was conducted in [4] for analyzing propagation in a small office at 300 GHz frequency band. Similar campaign with one-sided angular information is reported in [5]. Estimated parameters include angular spreads, delay spreads, K-factors, and identification of individual propagation paths. Desktop measurements without angular information are introduced in [6] and [7]. Some probability distributions for stochastic modelling, e.g., for shadowing and path loss, are extracted in [6].

The expectation is that the signal propagation at upper mm-wave and THz frequency is rather deterministic and follows well established formulas of transmission, reflection, and diffraction. It has been shown that ray tracing channel modeling methods provide good prediction capabilities at 60 GHz [8], and the same behaviour is anticipated at 0.3 THz frequency. Hence, the aim is to collect measurement based evidence to evaluate the expectations. In this work, we present the initial results of the propagation measurements at 220–330 GHz in the specific case when a small object such as human finger is blocking a LOS link. We use static, non-rotating Tx and Rx units with horn antennas and a three-axis positioner to move an object between the antennas. In other words, instead of moving the antennas, we move the object. The purpose is to evaluate the effects of a finger and other objects on the vicinity of antennas in conditions that could possibly occur during the usage of 6G device, e.g., the finger of the user is close to a frame of virtual reality glasses with integrated 6G radio or an edge of a laptop screen containing integrated 6G antennas. We got partial inspiration for the study from publications [9] and [10]. In the former, the finger effect on the 60 GHz antenna was investigated with an electro magnetic

(EM) simulator. The latter describes a 60 GHz measurement of the human body crossing a static LOS path, and it also proposes a model for the shadowing and scattering effect.

The higher operating frequency of the system denotes a shorter wavelength. The severity of the blocking effect on the system performance relates to the size of the obstacle measured in wavelengths. A human finger of 1.5 cm at 300 GHz corresponds to 15 wavelengths. The same 15 wavelengths electrical size at 39, 2, 1, and 0.7 GHz corresponds to the size of a hand palm, a small city car, a mid-size car, and a large van, respectively. Sizes of physical objects with a similarly significant effect on the radio link performance are scaled-down when the radio link's operational frequency increases.

II. Methods

In the following subsections we describe the measurement system and discuss briefly the processing and theories used in evaluations.

A. Measurement System

A block chart of the measurement setup is shown in Fig. 1. The setup consist of four-port Keysight N5242B vector network analyzer (VNA) connected to transceiver (TRx) and Rx frequency extenders by Virginia Diodes Inc. (VDI). The Tx extender is connected to VNA ports 1 and 3 and the Rx extender is connected to VNA ports 2 and 4. Ports 1 and 2 operates at fixed frequency of 279 MHz and ports 3 and 4 sweeps the local oscillator (LO) from around 9.16 to 13.74 GHz. The RF at the Tx extender output and Rx extender input are swept from 220 GHz to 330 GHz. WR3.4 standard gain horn antennas are used at Tx and Rx. The gain of the antennas is around 20.5 dB with 15 degree bandwidth in E and H-planes. The measurement setup is calibrated by using enhanced response calibration from the Tx to the Rx extender due to the fact that the used Rx is not capable of using full thru-line-reflect (TLR) calibration.

Fig. 2 is a photograph taken on top of the Rx antenna. The Rx horn is opposite to Tx at a distance of 350 mm and is not shown in the photograph. The three-dimensional (3D) positioner controlled by stepper motors is used to move the object in front of the Tx extender. The positioner and VNA are controlled by Matlab-based control software for enabling fully automated measurements. The origin of the coordinate system is on the Tx antenna. The axis perpendicular to the Tx-Rx line is labelled as Y and the parallel axis is labelled as X. The used motion range on Y and X axes are $-50 \ldots 50$ mm and $5 \ldots 165$ mm, respectively, with minimum increment of 1 mm.

Fig. 3 depicts an example of the measured channel transfer function without the blocking objects. It is composed of the free space loss, ranging from 70 to 74 dB, and antenna gains ranging from 19 to 22 dB on the measurement band. With identical horn antennas at both link ends, this sums up to approximately -30 dB path gain that is readable from Fig. 3. With a fixed aperture at both link ends, the total antenna gain over-compensates the rise of free space loss,

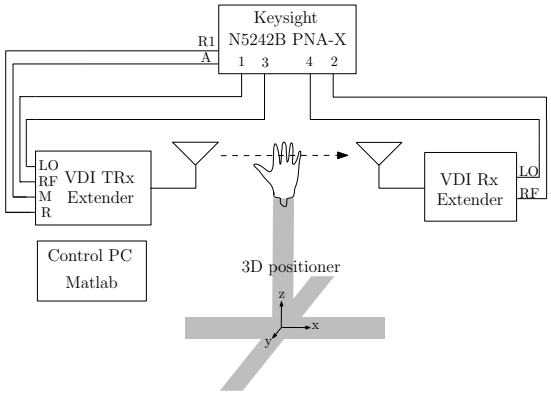

Fig. 1. Block chart of the measurement setup. The link-blocking object is moved by the 3D linear positioner between the fixed Tx and Rx antennas.

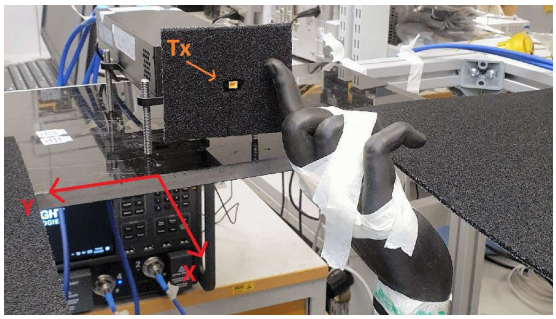

Fig. 2. Photograph of the hand measurement. Coordinate axes are illustrated with red arrows.

as can be observed from the slightly increasing the trend of transfer function in Fig. 3. The few decibel fluctuation of the measurement is explained by signal reflections that were not to fully attenuated by the absorbers, as shown in Fig. 2.

With the measurement bandwidth of 110 GHz the achievable delay resolution is approximately 9.1 ps. In distance this correspond to propagation length resolution of 2.7 mm.

We recognize that the phantom hand used in the measurements is intended for below 6 GHz and not for the investigated frequencies. However, we expect that a real finger has a very high absorption loss, and the primary propagation mechanism is diffraction on finger edges. We do not have phantom hand models available for THz frequencies, which is another research topic to develop such models.

It is noted that the positions of different objects are not perfectly comparable. The positioner itself has accuracy down to $\approx 10^{-5}$ mm, but the starting coordinates of the grid are changed slightly from object to object due to the mechanical attachment of the object to the 3D positioner. Hence, the origin of the coordinate system is set manually for each object.

B. Processing of the Measurement Data

VNA measures the forward scattering parameter (S-parameter) of the radio channel. Hence, the output of each measurement is a complex channel frequency response (CFR) $H(f, x, y)$ at certain object coordinates x, y and frequency

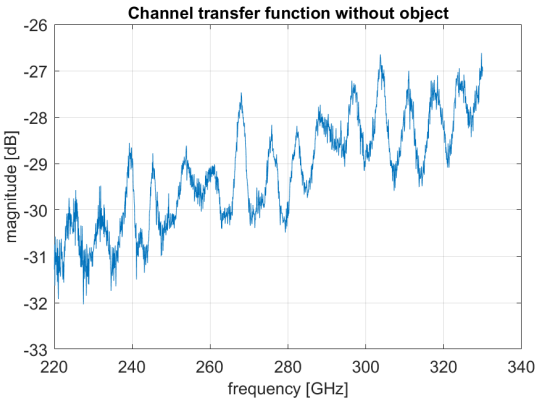

Fig. 3. Channel transfer function of the measurement system without a blocking object. The magnitude per frequency is composed of antenna gains minus the free space loss.

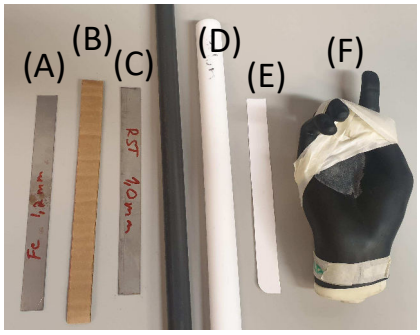

Fig. 4. Photograph of the objects under test listed as (A) iron strip, (B) corrugated cardboard strip, (C) stainless steel strip, (D) Nylon rod, (E) cardboard strip, and (F) phantom finger.

f. CFRs are converted to channel impulse responses (CIRs) $h(\tau, x, y)$ with the inverse Fourier transform, where τ denotes propagtion delay. An example CFR without an object is depicted in Fig. 3.

By using absorbers, we were able to block most of the reflections from the surroundings. However, there are multiple reflections between the object and the antennas, as well as between the antennas, that cannot be blocked in the measurements without affecting to the antenna operation. We studied the blockage and diffraction effects of different objects and their impacts on the channel gain. Thus, we filter out the (multiple) reflected paths by time gating the CIRs. The channel gain is determined as

$$G(x, y) = \Sigma_{\tau \in \tau_l} |h(\tau, x, y)|^2, \tag{1}$$

where τ_l is a set of delay bins close to the delay of the LOS path. A reflection from the Tx antenna will be counted on (1) when the object is closest to Tx, but similar reflections may be present also with real devices.

C. Theoretical tools

The concept of Fresnel zones can be used to assess the impact of a knife edge diffracting object. The nth Fresnel zone is an ellipsoid wherein the extra propagation length is $n\lambda/2$. It can be understood as containing the propagated energy of a wave. Radius of the nth ellipsoid is approximately

$$r_n = \sqrt{\frac{n\lambda d_1 d_2}{d_1 + d_2}}, \tag{2}$$

where d_1, d_2 and λ are the Tx-object distance, object-Rx distance and the wavelength, respectively [11]. If 60% of the first Fresnel zone is cleared the obstruction loss is zero. Radii of these clearance areas at the centre frequency of the measurement are 3, 6 and 13 mm for distances $x = 5$, 21 and 165 mm, respectively.

The phase velocity of EM waves varies in different media. The higher the relative permeability μ_r and permittivity ϵ_r, the lower the velocity. The refractive index

$$n = \sqrt{\mu_r \epsilon_r} \tag{3}$$

determines the ratio of phase velocities in the free space and in the medium [11].

III. Results

The six objects shown in Fig. 4 were measured. The objects are a phantom hand made of a silicone-carbon mixture, two metallic stripes, two cardboard stripes, and a rod made of Nylon. Their dimensions, width $\times$ thickness for stripes and diameter for the rod, are defined in Table I. The thin cardboard strip is coated on one side and is matt finished on the other side. The corrugated cardboard has thin cardboard layers on both sides and a corrugated layer in between. The corrugations are horizontally oriented. The orientation of the phantom hand is shown in Fig. 2, where the index finger is not perfectly straight. All stripes were vertically oriented, such that broad sides are facing Tx and Rx. The rod is a rotationally symmetric solid bar, and its axis was vertically oriented. We do not know complete dielectric characteristics of the objects for the considered frequency, not even from the literature.

Results can be analyzed over various dimensions. CIRs of four objects at $x = 5$ mm and y between –40 and 40 mm are visualized in Fig. 5. The blockage effect is visible in the Figs. 5 (a) to (d), when $y = 0$. For phantom finger in (a), the CIRs show a peak at 351 mm propagation length, but the peak is 51 dB attenuated as compared to the no object case. Also the stainless steel strip in (b) has strong attenuations in $y = 0$. The corrugated cardboard strip in (c) shows diffraction on edges, but the wave penetrates the material with only 1.2 dB loss compared to the free space. The Nylon rod in Fig. 5 (d) shows an interesting phenomenon. When the rod is in the direct link chord, the strongest peak of the CIRs is delayed. This is due to the slower speed of the wave at Nylon compared to the free space as defined by (3). Moreover, the strength of the signal is increased in this point due the collimating impact of the rod, and the focus point is clearly visible at $y = 0$. Thus, the Nylon rod acts as a lens at 220-330 GHz frequencies. This observation is important to take into account when studying

the wave propagation at higher frequencies. The impact of iron strip was very similar to the stainless steel strip in Fig. 5 (b), and the cardboard was similar to the corrugated cardboard in Fig. 5 (c). Hence, those are left out from Fig. 5.

Normalized channel gains as a function of the xy-position are shown in Fig. 6 for the same objects as in Fig. 5. The normalization is performed by dividing the CFR at each object position by the CFR measured without the object. In Fig. 6 (a), the positions approximately between y =–40 and –25 mm are cases where the finger or the hand do not distract the transmitted signal. There the gain is similar to the free space path loss. On the positive y values between 20 and 40 mm we can observe increase of gain, especially when x increases and the hand is farther away from Tx. This probably results from interactions with other fingers of the phantom hand. The highest excess attenuation, 44 dB (best observable in Fig. 7), occurs when the finger is closest to Tx, i.e., in $y = 0$ and $x = 5$ mm. At $x = 21$ mm it is still 30 dB. Fairly clear diffraction patterns can be observed at y positions between –25 and –10 mm in all sub-figures. Excess attenuations of objects are listed in Table I. The *centre* column is for position $(x, y) =$ (5,0) mm and the *max* column values are from a position that maximizes the attenuation with the particular object.

Channel gains of all six objects are compared in Fig. 7. Distance x from Tx plane is 5 mm and the y position is swept from –40 to 40 mm. Metallic stripes yield similar U-shaped gain patterns as the finger. On one hand it is surprising, since their CIRs are dissimilar, but on the other hand it reflects our initial hypothesis. Namely, we assumed that the penetration loss of a (real) finger is high and the main contribution comes from edge diffractions.

In the case of metallic stripes the Fresnel zone clearance approximation has a good match with measurements. In Fig. 7 the gain starts dropping at $y = -12$ mm position. It is the position when the edge of 18 mm wide stripe penetrates the clearance zone at $y = -3$ mm. With the 26 mm wide Nylon rod the gain is still high at $y = -16$ mm, but begins to decrease at –15 mm. The finger is not straight and symmetric, thus the obstruction phenomenon is not that clearly readable from Fig. 7. The cardboard objects are farther from assumptions of single knife-edge attenuation, and do not renew the 0.6 clearance rule.

Cardboard stripes cause only small excess attenuation of 1.5 dB when closest to the Tx. The maximum excess attenuation of 4.4 and 6.4 dB with the normal and corrugated cardboard, respectively, occurs at $y = \pm$ 10 mm position. This is a condition when Rx is changed from the shadow of the strip to the illuminated region. Interestingly, even though the transmission loss is low, the diffraction pattern causes noticeable attenuations. If observing more closely the CIR of corrugated cardboard strip, the few paths at 351 mm and later, are just attenuated the mentioned 6 dB and the diffraction phenomenon is not resolvable in delay domain.

The Nylon rod may provide positive excess gain. The gain in $y = 0$ mm position is -25.8 dB while in $y = 5$ mm it goes down to -69.2 dB. In the latter position the rod lens is focusing signals off the direction of Rx. We can remark that the rod and possibly objects such as water bottles, knife handles and kitchen storage boxes may cause high variation onto the channel gain with only few mm displacement, if they are in the close vicinity of antennas. At 5 mm distance the gain variation was 43.4 dB, at distance up to 37 mm the variation is still up to 12 dB, and at 69 mm and longer the variation decreases below 4 dB.

TABLE I
MEASURED OBJECTS, THEIR DIMENSIONS AND THE EXCESS ATTENUATION BOTH IN THE CLOSEST POSITION TO TX AND THE MAXIMUM ATTENUATION POSITION.

Object	Dimensions [mm]	Attenuation centre [dB]	Attenuation max [dB]
Phantom finger	17×14	44.2	44.2
Iron strip	18×1.2	41.5	43.0
Stainless steel strip	18×1.0	39.3	39.3
Cardboard strip	18×0.3	1.5	4.4
Corrugated cardboard strip	18×3.5	1.6	6.5
Nylon rod	Ø 26	-3.8	39.6

IV. DISCUSSION

We are building propagation measurement capability at the University of Oulu, and in this paper, we analyze preliminary measurements performed with the setup at 220-330 GHz. A finger and other objects were moved across the LOS path at different distances from Tx. We found that the phantom finger may cause attenuation up to 44 dB. Even a displacement of a few millimeters may cause more than ten dB variation on the channel gain. The attenuation becomes milder with increasing distance from the antenna. However, the first Fresnel zones are less than 22 mm at the considered link distance, and they are easily blocked even by a finger-size objects.

The observations are as expected and emphasize the well-known principles of EM propagation theory. The finger and metallic stripes, e.g., yield similar gains with clear diffraction patterns. Cardboard stripes are almost transparent but still provide significant diffraction from their edges. Nylon rod, being an object of low loss material, acts as a lens magnifying the signal on certain positions, but causing high attenuation by refracting the signal on another position.

Shapes, position, and orientations of objects made of low loss materials have potentially a high impact on the channel gain. Interestingly, they can also focus and direct the transmitted signals, i.e., act as lenses, as we can clearly remark from the Nylon rod case. Some common objects such as bottles, kitchenware, and office supplies may cause similar effects on communication links at upper mm-wave and THz frequencies. The networks planning or radio resource management (RRM) operations in the future 6G networks must be extremely dynamic, even if transceivers are static, and only positions of small scale objects in the environment are changing.

For future studies, we leave the actual modeling or fitting of existing models onto the observed phenomena. Further

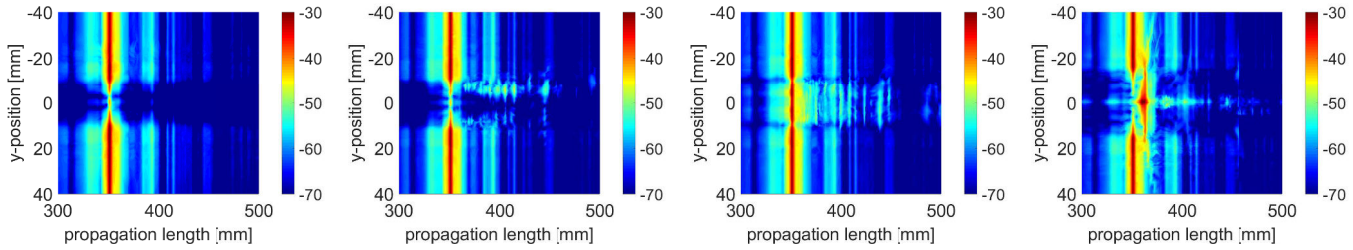

Fig. 5. Measured CIRs at versus the object y-position with (a) phantom finger, (b) stainless steel strip, (c) corrugated cardboard strip, and (d) Nylon rod as an object. The zero-position is selected such that the object is at the direct link chord at 5 mm distance from Tx.

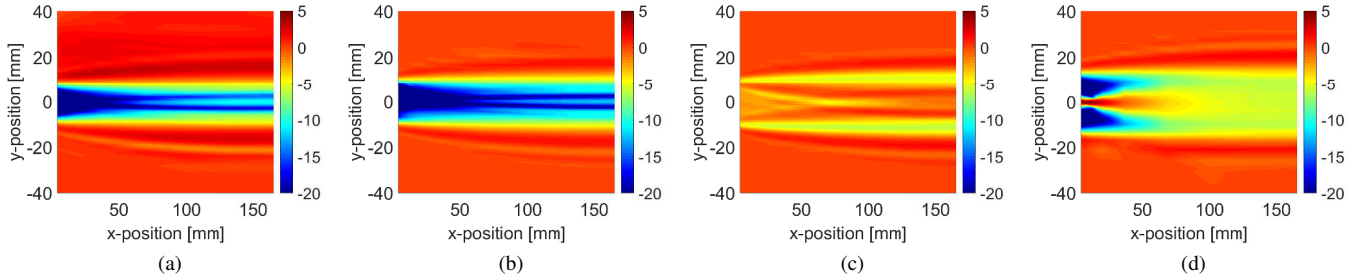

Fig. 6. Normalized channel gain versus the 2D position with (a) phantom finger, (b) stainless steel strip, (c) corrugated cardboard strip, and (d) Nylon rod as the object.

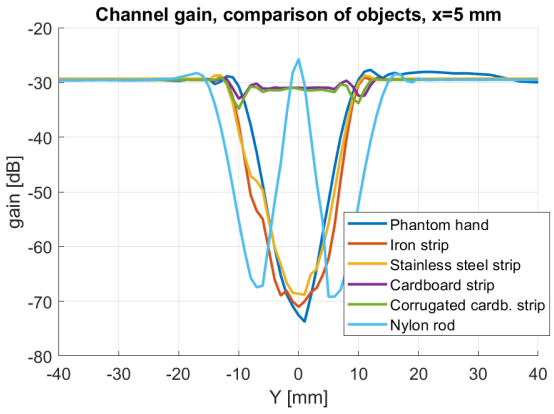

Fig. 7. Channel gains with all objects at positions $x = 5$ mm and $y = -40 \ldots 40$ mm.

research would be done on the usability of our measurement setup for material and structural characterization of low loss materials. The development of the hand and other phantoms for higher frequencies is also a topic for future research.

Acknowledgment

This work has been done in 6G Flagship programme, funded by Academy of Finland (grant no. 318927), in 5G Viima project, and in the H2020 project Hexa-X funded by the EC (Grant Agreement no. 101015956). Thanks to Keysight Technologies for measurement equipment. Thanks to Miia Nurkkala, Verkotan Oy, for the phantom hand.

References

[1] M. Latva-aho and K. Leppänen (eds.), "Key drivers and research challenges for 6G ubiquitous wireless intelligence," White paper, September 2019.

[2] IEEE 802.15.3d, "IEEE Standard for high data rate wireless multi-media networks - amendment 2: 100 Gb/s wireless switched point-to-point physical layer," IEEE, Tech. Rep., September 2017.

[3] S. Salous, V. Degli Esposti, F. Fuschini, R. S. Thomä, R. Müller, D. Dupleich, K. Haneda, J. Molina Garcia-Pardo, J. Pascual Garcia, D. P. Gaillot, S. Hur, and M. Nekovee, "Millimeter-wave propagation: Characterization and modeling toward fifth-generation systems. [wireless corner]," *IEEE Antennas and Propagation Magazine*, vol. 58, no. 6, pp. 115–127, 2016.

[4] S. Priebe, M. Kannicht, M. Jacob, and T. Kürner, "Ultra broadband indoor channel measurements and calibrated ray tracing propagation modeling at THz frequencies," *Journal of Communications and Networks*, vol. 15, no. 6, pp. 547–558, 2013.

[5] Z. Yu, Y. Chen, G. Wang, W. Gao, and C. Han, "Wideband channel measurements and temporal-spatial analysis for terahertz indoor communications," in *2020 IEEE International Conference on Communications Workshops (ICC Workshops)*, 2020.

[6] S. Kim and A. G. Zajić, "Statistical characterization of 300-GHz propagation on a desktop," *IEEE Transactions on Vehicular Technology*, vol. 64, no. 8, pp. 3330–3338, 2015.

[7] Y. Zantah, M. Alissa, T. Kreul, and T. Kaiser, "Ultra-wideband multipath channel characterization at 300 ghz," in *WSA 2020; 24th International ITG Workshop on Smart Antennas*, 2020, pp. 1–5.

[8] T. Kürner and S. Priebe, "THz Communications - Status in Research, Standardization and Regulation," *Journal of Infrared, Millimeter, and Terahertz Waves*, vol. 35, pp. 53–62, January 2014.

[9] M. Heino, C. Icheln, and K. Haneda, "Finger effect on 60 GHz user device antennas," in *2016 10th European Conference on Antennas and Propagation (EuCAP)*, April 2016.

[10] J. Medbo and F. Harrysson, "Channel modeling for the stationary UE scenario," in *7th European Conference on Antennas and Propagation (EuCAP 2013)*, April 2013, pp. 2811–2815.

[11] S. R. Saunders, *Antennas and Propagation for Wireless Communication Systems*. John Wiley & Sons, Ltd, Chichester, England, 1999, 409 p.